Journal of Materials Chemistry A

Layered Transition Metal Oxyhydroxides as Tri-functional Electrocatalysts

Journal:	*Journal of Materials Chemistry A*
Manuscript ID:	TA-ART-03-2015-002063.R1
Article Type:	Paper
Date Submitted by the Author:	22-Apr-2015
Complete List of Authors:	Lim, Chee Shan; Nanyang Technological University, Chemistry and Biological Chemistry Chua, Chun Kiang; Nanyang Technological University, Chemistry and Biological Chemistry Sofer, Zdenek; Institute of Chemical Technology, Prague, Department of Inorganic Chemistry Klimova, Katerina; Institute of Chemical Technology, Prague, Department of Inorganic Chemistry Boothroyd, Chris; Forschungszentrum Jülich, Ernst Ruska-Centrum Pumera, Martin; Nanyang Technological University, Chemistry and Biological Chemistry

Journal Name

RSCPublishing

ARTICLE

Layered Transition Metal Oxyhydroxides as Tri-functional Electrocatalysts

Cite this: DOI: 10.1039/x0xx00000x

Chee Shan Lim[a], Chun Kiang Chua[a], Zdeněk Sofer[b], Kateřina Klímová[b], Christopher Boothroyd[c], Martin Pumera*[a]

Received 00th January 2012,
Accepted 00th January 2012

DOI: 10.1039/x0xx00000x

www.rsc.org/

Layered transition metal-based materials have been intensively explored for their electrocatalytic capabilities in energy-related applications such as hydrogen evolution (HER) and oxygen evolution (OER) lately. These reactions are kinetically sluggish, and require catalysts to promote their efficiency. Since their discovery and characterization decades ago, the catalytic properties of metal oxyhydroxides have not been profoundly studied. It was only in recent years when emphasis was placed back on them again, mainly as possible OER catalysts. In this work, we wish to delve deeper into a several layered first-row transition metal (cobalt, chromium, iron, manganese and nickel) oxyhydroxides, and investigate their inherent electrochemistry and their electrocatalytic behaviors for HER and OER, as well as oxygen reduction reaction (ORR). Characterisation of these materials was performed with scanning electron microscopy, X-ray powder diffraction, high resolution transmission electron microscopy and X-ray photoelectron spectroscopy prior to the electrochemical studies. Among the five layered oxyhydroxides examined, cobalt and nickel oxyhydroxides proved to exhibit better electrocatalytic properties than the other three layered oxyhydroxides mainly in HER and OER.

1. Introduction

For many years, fossil fuels have been a key source of energy storage and production. However, increasing demand of fossil fuels to feed the energy needs of the growing population, coupled with emissions of carbon dioxide gases from fossil fuel combustion has sparked rigorous attempts to discover renewable and environment-friendly alternatives.[1,2] Electrochemical and photoelectrochemical splitting of water is amongst the most promising means to generate hydrogen and oxygen for storage of solar energy today.[3,4] It is a clean method of energy generation, with no harmful by-products given off during the process.[5] Despite its great benefits, the sluggish kinetics of the two processes involved, hydrogen evolution (HER) and oxygen evolution (OER) have hindered the efficiency of this method. It is therefore imperative to develop useful catalysts with high efficacy and stability for the enhancement of the reaction kinetics of hydrogen and oxygen evolution.

Precious metal catalysts, in particular platinum,[6,7] iridium and ruthenium5[,8] are known to be peerless in catalyzing HER and OER respectively, providing electrode surfaces capable of achieving large current densities at low overpotentials. However, despite their outstanding electrocatalytic abilities, large-scale usage of these catalysts remains greatly hindered due to the high cost and low abundance of these metals. Development of alternative active electrocatalysts using earth-abundant materials becomes a continuous challenge as such. Transition metals-based materials and composites have been studied and introduced as potential replacements of platinum and ruthenium lately. Hydrogenases comprising of cheaper metals such as nickel and iron as well as transition metal chalcogenides were proposed as HER catalysts,[9,10] while alloys and oxides involving manganese,[11] nickel[12] and especially cobalt[13,14] have been deemed suitable as OER catalysts.

Layered materials have been in the frontiers of materials chemistry research and their potentials have been extensively investigated lately.[15,16] Amongst the layered materials is a group of layered transition metal oxyhydroxides, with a chemical formula of MO(OH), with M representing the transition metal. The structures and properties of some layered oxyhydroxides such as nickel oxyhydroxide and iron oxyhydroxide have been investigated decades ago,[17,18] but it is only in the recent years that emphasis has been placed on their electrocatalytic abilities.[19,20,12] Recent studies have shown that various layered metal oxyhydroxides including that of iron and cobalt, as well as hybrid oxyhydroxides possess impressive electrocatalytic performances towards oxygen evolution.[21-24] Such is a testament of the stability of layered oxyhydroxides in alkaline medium. On the contrary, limited effort was focused

on the electrocatalytic activity of these layered oxyhydroxides in acidic medium for hydrogen evolution. In this work, we synthesized and characterized five layered transition-metal oxyhydroxides, namely cobalt (CoO(OH)), chromium (CrO(OH)), iron (FeO(OH)), manganese (MnO(OH)) and nickel (NiO(OH)) oxyhydroxides. Subsequently, we explored their potential capabilities in HER and OER, before carrying out studies on their electrocatalytic behaviours in another important application of tantamount importance in the development of fuel cells and zinc- and lithium-air batteries,[25,26] oxygen reduction reaction (ORR).

2. Experimental

2.1 Materials

Nafion 117 solution, ethanol, platinum on graphitized carbon, sulfuric acid (55-98 %, v/v), potassium hydroxide, sodium chloride, potassium chloride, sodium phosphate dibasic and potassium phosphate monobasic were purchased from Sigma-Aldrich, Singapore. Chromium nitrate nonahydrate, manganese sulfate tetrahydrate, iron(II) chloride tetrahydrate, cobalt nitrate hexahydrate, nickel nitrate hexahydrate, bromine, hydrogen peroxide (30 wt.%), ammonia (25 wt.%) and potassium hydroxide were obtained from Penta, Czech Republic. Argon of 99.996% purity was obtained from SIAD, Czech Republic. Glassy carbon (GC) electrodes with a diameter of 3 mm was obtained from Autolab, The Netherlands. The modulated speed rotator set-up (model PGSTAT302M) and the rotating-ring disk electrode (RRDE) with a diameter of 5.6 mm were obtained from Pine, Durham, USA. Milli-Q water with a resistivity of 18.2 MΩcm was used throughout the experiments.

2.2 Instrumentation

X-ray photoelectron spectroscopy (XPS) measurements were recorded using a Phoibos 100 spectrometer and a monochromatic Mg X-ray radiation source (SPECS, Germany). Survey scans and high-resolution spectra of the layered oxyhydroxides and C1s were measured to understand the chemical bonding within the materials. Preparation of the samples was done by sticking the material onto an aluminium XPS sample holder using a sticky conductive carbon tape. The layer of material was ensured to be uniform throughout. Scanning electron microscopy (SEM) was carried out with Jeol 7600F SEM (Jeol, Japan) operating at 2 kV in GB high to study the morphology of the materials. Energy-dispersive X-ray spectroscopy (EDS) was measured on a Jeol 7600F (Jeol, Japan) at 15 kV to acquire the mapping and elemental composition of the layered oxyhydroxides. Typical error of EDX measurements is about 5%. High resolution transmission electron microscopy (HRTEM) images were taken using a FEI Titan "Holo" G2 60-300 field emission gun transmission microscope. The sample suspension (1 mg/mL) was dropped onto a lacy carbon grid. A Gatan UltraScan 1000 2k CCD camera was used acquire images. The EEL spectra were acquired using a Gatan imaging filter (Tridiem ER model 865) attached to the same microscope. X-ray powder diffraction data were collected at room temperature with an X'Pert PRO θ-θ powder diffractometer with parafocusing Bragg-Brentano geometry using $Cu_{K\alpha}$ radiation (λ = 0.15418 nm, U = 40 kV, I = 30 mA). Data were scanned with an ultrafast detector X'Celerator over the angular range 5-80° (2θ) with a step size of 0.0167° (2θ) and a counting time of 20.32 s $step^{-1}$. Data evaluation was performed in the software package HighScore Plus 3.0e.

Linear sweep voltammetry (LSV) and cyclic voltammetry (CV) measurements were recorded with a μAutolab type III electrochemical analyser (Eco Chemie, The Netherlands) connected to a personal computer and controlled by NOVA 1.8 software. HER and ORR experiments were performed in a 5 mL electrochemical cell with GC electrodes while OER experiments in a 200 mL electrochemical cell with a RRDE; all measurements were performed at room temperature using a three-electrode configuration. A platinum electrode functioned as an auxiliary electrode while an Ag/AgCl electrode was utilised as a reference electrode. Rotation speed of RRDE for OER measurements was kept constant at 500 rpm. All electrochemical potentials in this paper are stated *vs.* the Ag/AgCl reference electrode unless otherwise stated in the figures.

2.3 Procedure

Synthesis of CoO(OH): A solution of 14 g of KOH in 75 mL of H_2O was added drop wise (under stirring) to a solution of 22.5 g of $Co(NO_3)_2{\cdot}6H_2O$ and 3 mL of Br_2 in 325 mL. The resulting precipitate settles in about three hours. It was washed by decantation with five 2.5 L portions of CO_2-free DI water. The precipitate is slurred in 1 L of DI water. The slurry was centrifuged (5000 rpm, 30 mins) and the solid was dried in vacuum oven (50 °C, 48 hrs). All operations must be carried out in a CO_2-free atmosphere.

Synthesis of CrO(OH): 15 g of $Cr(NO_3)_3{\cdot}9H_2O$ was dissolved in 75 mL of DI water. 10% solution of ammonia was added drop wise under continuous stirring and pH measurement. Once pH 5.0 was gained the mixture was centrifuged (15 000 rpm, 10 min). The resulting solid was washed and centrifuged three times. The sediment was given to 25 ml beaker, which was placed in autoclave. 2 mL of DI water were added between Teflon vessel and beaker. The autoclave was putted to oven (170 °C) for 12 hours, next the solid was dried in vacuum oven (50 °C, 48 hrs).

Synthesis of FeO(OH): 10 g of $FeCl_2{\cdot}4H_2O$ was dissolved in 500 mL of CO_2-free deionized water (DI water). This solution was bubbled through by argon for 15 minutes. Then 100 mL of 0.1 M solution of KOH was added drop wise. Reaction mixture was then stirred for an hour. Solution of 8 g KOH with 2.5 mL of Br_2 dissolved in 50 mL of DI water was added dropwise. Reaction mixture was stirred for another hour. The resulting precipitate settles in about three hours. It was washed by decantation with five 2.5 L portions of CO_2-free DI water. The precipitate is slurred in 1 L of DI water. The slurry was

centrifuged (5000 rpm, 30 min) and the solid was dried in vacuum oven (50 °C, 48 hrs).

Synthesis of MnO(OH): 2.4 g of $MnSO_4 \cdot 4H_2O$ was dissolved in 300 mL of water and under vigorous agitation was added 34 mL of 3 wt% H_2O_2 solution. With continued stirring was added 50 mL of 0.2 M NH_3 solution. The black MnO(OH) suspension formed was boiled for 5 mins and subsequently removed by suction filtration and repeatedly washed with deionized water and dried in vacuum oven (50 °C, 48 hrs).

Synthesis of NiO(OH): A solution of 25 g of $Ni(NO_3)_2 \cdot 6H_2O$ in 375 mL of H_2O is added drop wise and with vigorous stirring to a solution of 13.75 g of KOH and 3 mL of Br_2 in 75 ml of H_2O. The precipitation temperature should not exceed 25 °C. The precipitate is washed five times (decantation) with CO_2-free H_2O. The wet product is dried in vacuum oven (50 °C, 48 hrs). All operations must be carried out in a CO_2-free atmosphere.

Cyclic voltammetry measurements were taken at a scan rate of 100 mV s^{-1} for inherent electrochemistry scans. Linear sweep voltammetry measurements were recorded at a scan rate of 2 mVs^{-1} for HER and OER, and 5 mV s^{-1} for ORR. HER was performed in 0.5 M sulfuric acid, whereas OER and ORR in 0.1 M potassium hydroxide. The reproducibility of the measurements was achieved by carrying out three replicates for each experiment.

Electrode surfaces were renewed by polishing with 0.05 μm alumina powder on a polishing pad. A suspension of the desired material with a concentration of 5 mg mL^{-1} in respective solvent mixtures was first prepared, followed by a 60 min ultrasonication. Suspension used for HER is a water-ethanol-nafion mixture in the ratio of 19:5:1 for every 250 μL solvent mixture; water suspension with 0.1 wt% nafion solution was used as the solvent for OER and ORR experiments. A micropipette was then used to deposit 1 μL aliquot (5 μL for OER due to larger electrode diameter) of the appropriate suspension onto the electrode surface to immobilise the material onto the working electrode. The solvent was allowed to evaporate at room temperature to obtain an evenly distributed film on the electrode surface.

3. Results and Discussion

Characterisation of the five layered oxyhydroxides was performed following the synthesis. The morphologies of the materials were firstly studied using scanning electron microscopy (SEM), to identify any structural differences among the five materials.

Morphology of the five layered oxyhydroxides at microscale were studied in **Figure 1**, and they vary in shapes and appearances. CoO(OH) displays irregular platelet-like structures ranging from 100 to more than 700 nm in length. CrO(OH) exhibits rounder particles coagulated together into larger round structures, with diameter particles observed to be as small as 50 nm. SEM image of FeO(OH), as shown in **Figure 1C**, depicts a relatively layered structure, though the layers still seemed stacked together. The structure of MnO(OH) differs from the rest, with long, thin strips of particles observed. The strips are of varied lengths and arranged in a random, disorganised manner. Finally, the structure of NiO(OH) resembles that of CrO(OH), the only difference being the larger extent of particle separation in the former from the clearer and more distinct particles detected. Energy-dispersive spectroscopy (EDX) was then carried out to detect presence of any impurities in the materials synthesized. The EDX spectra are displayed in **Figure S1** of Supporting Information, while the atomic percentage (at%) distribution in the five layered oxyhydroxides are tabulated in **Table 1**. Ideal stoichiometric ratio between the metal and oxygen should be 1:2, and the ratios attained for most materials concurred closely with this value.

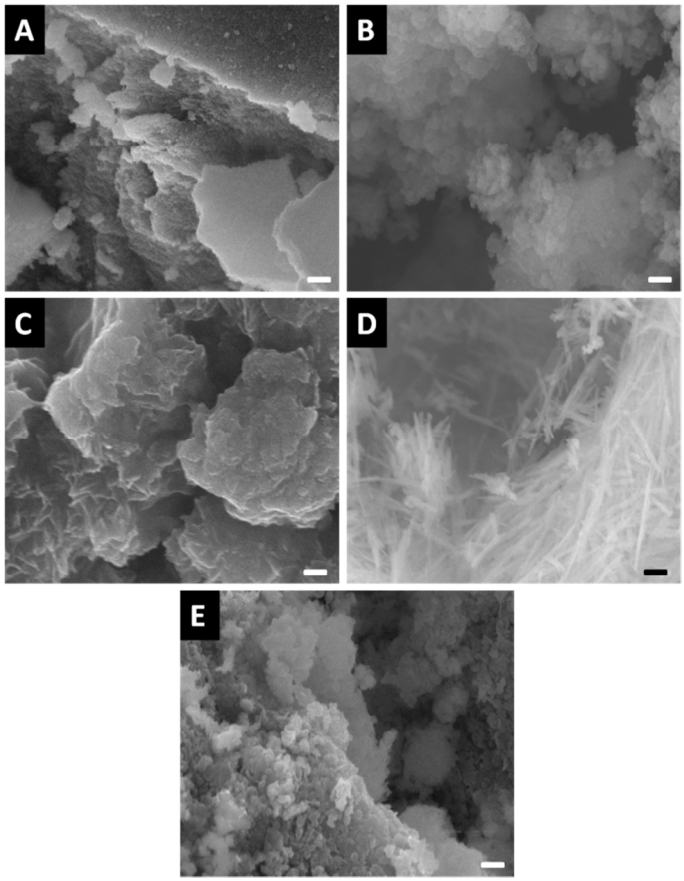

Figure 1 SEM images of (A) CoO(OH), (B) CrO(OH), (C) FeO(OH), (D) MnO(OH) and (E) NiO(OH) at magnifications of 40,000 x. Scale bars represent 200 nm.

Table 1 Summary of EDX Data for the five oxyhydroxides

Material	Atomic Percentage (at%)		Ratio of M:O
	M (M = metal)	O	
CoO(OH)	34.7	65.3	1:1.88
CrO(OH)	36.0	64.0	1:1.88
FeO(OH)	34.9	65.1	1:1.87
MnO(OH)	28.5	71.5	1:2.51
NiO(OH)	29.1	70.9	1:2.44

The material was further characterized using HR-TEM microscopy in combination with EELS for composition estimation. The TEM and HR-TEM images and corresponding EELS spectra are shown on **Figure 2**. The CoO(OH) composed

of very small plates with lateral size up to ten nanometers which are arranged in larger platelet aggregates. CrO(OH) is made up of platelet-like material, with lattice fringes observed

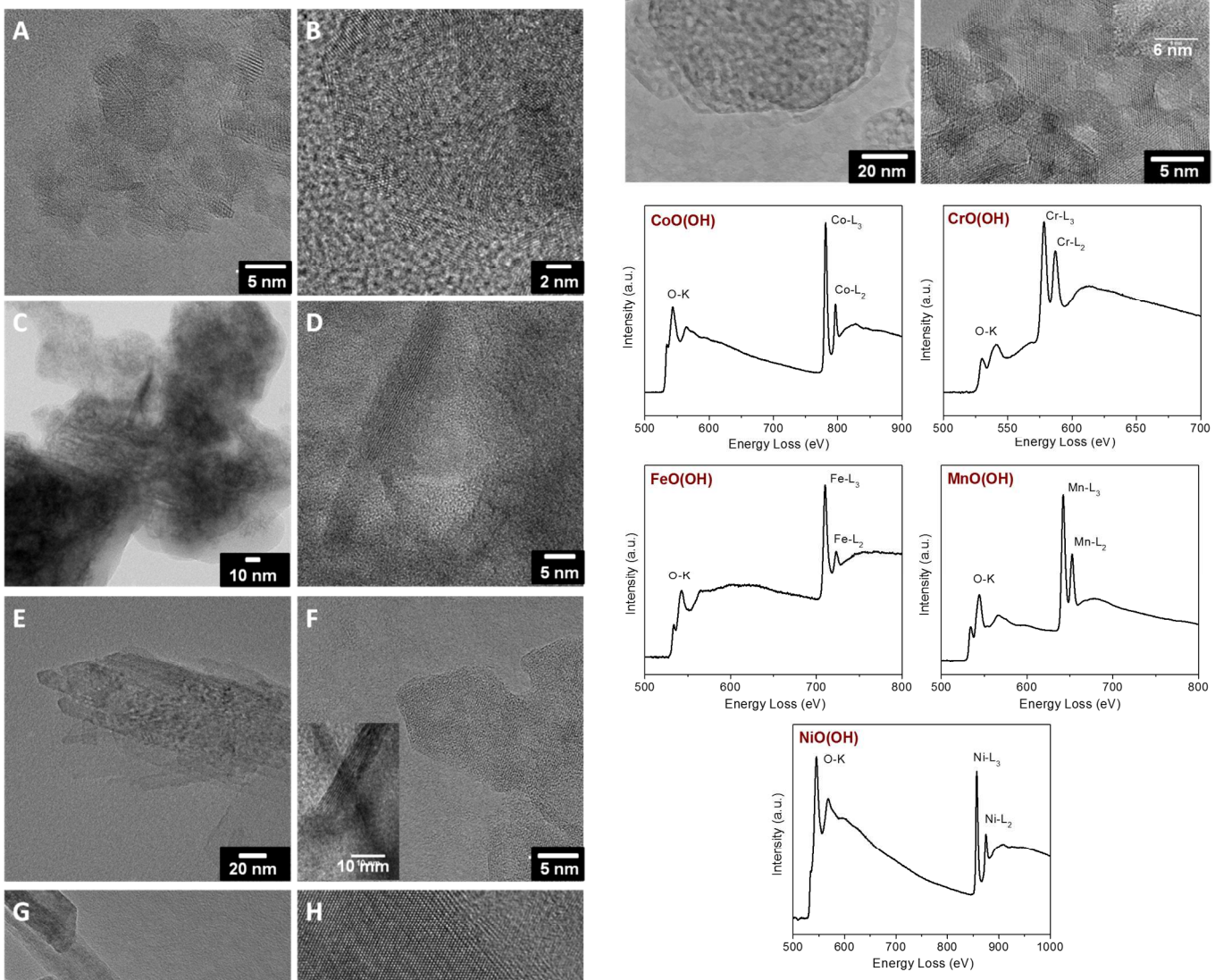

Figure 2 The HR-TEM images of (A, B) CoO(OH), (C, D) CrO(OH), (E, F) FeO(OH), (G, H) MnO(OH) and (I, J) NiO(OH) and their respective EELS spectra.

only on several particles. This corresponds to the results of X-ray diffraction which will be discussed further. Individual platelet particles have size from ten nanometers up to few hundred nanometers, while the thickness is about 5–10 nm. MnO(OH) exists in plates in one longitudinal direction with thickness about 5–10 nanometers and lateral size in the range of 10–40 nm. The length of observed was up to several hundred nanometers. Similar observation was concluded for FeO(OH) where the needle-like plates with thickness of several nanometers. The crystallinity was lower compared to MnO(OH). The last two oxyhydroxides have platelet-like shapes. NiO(OH) form significantly bigger particles with size up to 100 nm and thickness of 5–10 nm. These plate particles of hexagonal profile contain "hole–like" structures of nanometer size. Oxygen was also detected in all EELS spectra together

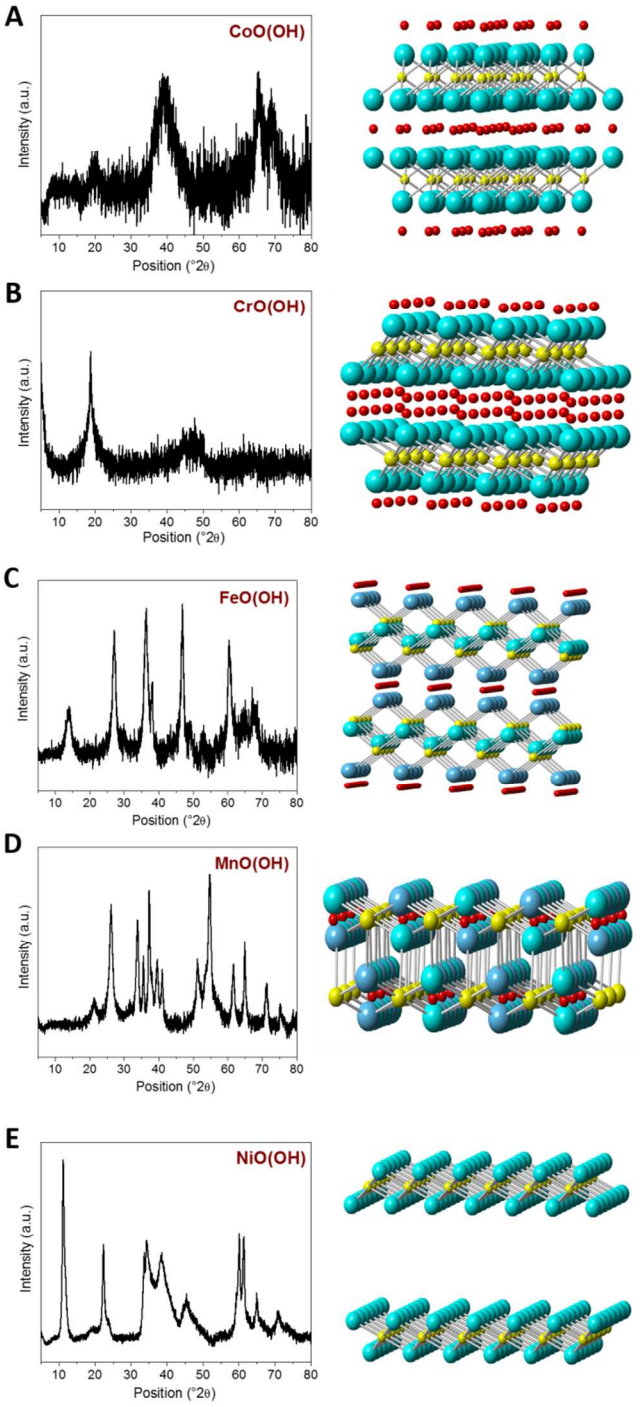

Figure 3 The X-ray diffraction of oxyhydroxides and corresponding model of structure. (blue – oxygen, red – hydrogen, yellow – metal).

with corresponding metal in all the metal oxyhydroxide samples.

The phase composition was investigated in detail using X-ray diffraction. The results of X-ray diffraction are shown on **Figure 3** together with the structure models of corresponding phase. The X-ray diffraction of the CoO(OH) sample shows presence of heterogenite, with the space group R-3m. High broadening of diffraction pattens corresponds to the crystallite size of 5 nm. This is in perfect agreement with the HR-TEM images where was observed small platelet crystals with size about 5 nm agglomerated to larger particles.

The CrO(OH) sample shows the presence of rhombohedral phase (space group R-3m) with low degree of crystallinity where only diffraction line 19.91 °2θ corresponding to (003) reflection was clearly visible. The broadening of (003) reflection corresponds to the plate thickness of about 6 nm. This concurs with HR-TEM observations. The X-ray diffraction of FeO(OH) illustrates presence of pure orthorombic phase (space group Cmc21) known as lepidocrocoite, γ-FeO(OH) phase. The broadening of diffraction patern indicates presence of small crystallites with sizes up to 10 nm. This matches the HR-TEM images where high disorter was observed with platelet thickness about 10 nm. The MnO(OH) diffraction pattern reveals the existence of a monoclinic phase (space group P21/c) known as manganite (γ-MnO(OH)). Diffraction pattern broadening corresponds to a crystallite size of about 8 nm. Presence of a mixed hydroxide-oxyhydroxide with hexagonal structure and formula $3Ni(OH)_2 \cdot NiO(OH)$ was detected for the final sample. This finding agrees with the deconvolution of the high resolution XPS spectrum for Ni 2p, where presence of Ni^{2+}/Ni^{3+} mixed valence state was also proved.

Upon determining the morphologies of the oxyhydroxides, XPS was carried out on the materials and analysis was done on the M 2p (M denotes the respective metals) and O 1s high resolution spectra, as exemplified in **Figure 4**.

CoO(OH) Figure 4A shows the high resolution spectra for cobalt oxyhydroxide. For the Co 2p spectrum, the most intense $2p_{3/2}$ peak representing the Co^{3+} ion occurs at 778.8 eV; this value matches closely with previous studies on this material.[27,28] The presence of a second $2p_{3/2}$ peak at about 780.9 eV also corresponds very closely to literature value of 781.7 eV, with a slight shift to lower binding energy. The first and second peaks are attributed to the Co–O and Co–O–H environments respectively. A telling sign of Co(III) oxides using XPS is the absence of multielectron excitation satellite peaks, which is generally present in Co (II).[27] Trace amounts of Co^{2+} might have existed in the CoO(OH) sample owing to a small absence located at around 784.8 eV, which is commonly found in $Co(OH)_2$ (~786 eV). The final peak at around 788 eV indicates a lower satellite peak, which is usually retained by both Co(II) and Co(III) oxides. Similar to literature, four peaks were fitted for the O 1s spectrum. Two most intense peaks at 528.7 and 529.9 eV represent the oxygen from the O^{2-} and OH^- portions, with the hydroxide ions positioned at the higher binding energy side.[29] It is also apparent that these two peaks are in similar ratio quantitatively, consistent with their 1:1 atom ratio.

CrO(OH) The XPS high resolution spectra for CrO(OH) are displayed in Figure 4B. Two broad envelopes at approximately 586 and 576 eV in the Cr 2p spectrum represent the $2p_{1/2}$ and $2p_{3/2}$ signals respectively. These peak positions concur with that

in earlier studies, where the $2p_{3/2}$ peaks at 575.5 and 577.0 eV coincide with that of trivalent oxides and hydroxides respectively.[30,31] Absence of a broad signal at a slightly binding energy of 579 eV indicates negligible amounts of Cr (III) free ions in the material synthesized. The spin-orbit splitting of 9.7 eV is well in correspondence with the range between 9.7–9.9 eV observed by Allen *et. al.* in Cr^{3+} compounds.[32] As for the O 1s spectrum, the first peak at 529.8 eV also matches closely to that of literature value (530.2 eV) which represents the O^{2-} while the more significant peak at higher binding energy of 531.0 eV corresponds to that of OH^-. The final third peak at about 532.3 eV, on the other hand, is symbolic of oxygen in water.[31] This can indicate the presence of an amorphous phase such as $Cr(OH)_3.xH_2O$or complex hydrated hydroxide $[Cr(OH)_3(H_2O)_3.3H_2O]$. As the O^{2-} and OH^- peaks exist in equal abundance of about 45 % each, implying that the material existed largely as CrO(OH).

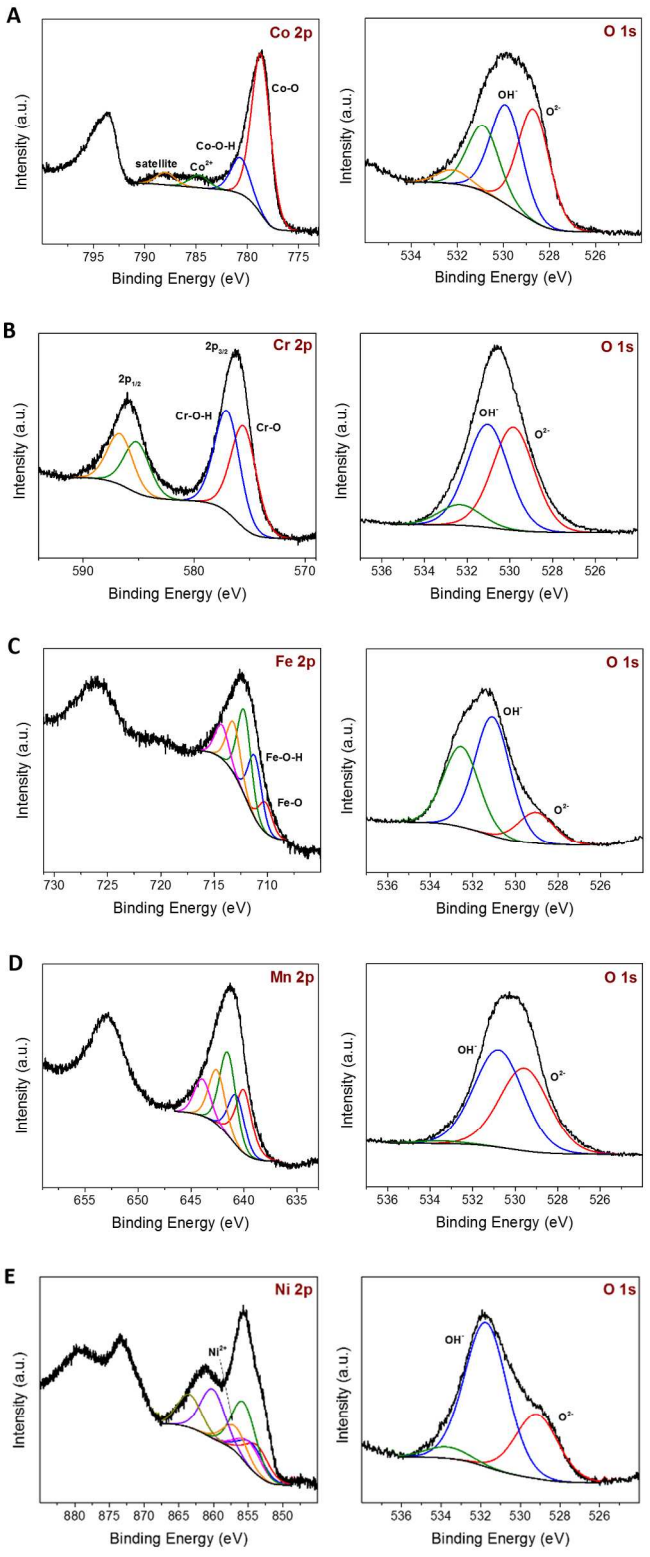

Figure 4 XPS high resolution (left panel) M 2p and (right panel) O 1s spectra of (A) CoO(OH), (B) CrO(OH), (C) FeO(OH), (D) MnO(OH) and (E) NiO(OH) respectively.

FeO(OH) The XPS spectra of the synthesized γ-FeO(OH) was analysed in Figure 4C. Five $2p_{3/2}$ peaks were fitted in the Fe 2p spectrum, ranging from 710.2 to 714.3 eV. Positions of these peaks match those proposed in previous studies, with only a slight difference of about 0.1 eV.[33–35] Amongst the peaks, the first peak at about 710.2 eV corresponds to Fe (III) oxides, whereas the peak at 711.2 eV represents that of Fe (III) hydroxides as documented by earlier studies.[36] As the mean peak position falls around 712 eV, the material synthesized was distinguished from Fe_2O_3 which exhibits an average peak at 711 eV.[35] Three peaks were also observed for the O 1s spectrum, with indicative peaks at 529 and 531.1 eV for the oxide and hydroxide environments respectively. A third peak at 532.5 eV can be attributed to possible adsorbed water in the material, as proposed by literature.[37,36]

MnO(OH) Figure 4D illustrates the spectra for Mn 2p and its corresponding O 1s in high resolution. Fitting of the Mn 2p spectrum was first established using the Mn^{3+} free ion spectra proposed by Gupta and Sen;[38] the mean binding energy for the $2p_{3/2}$ signal occurs at about 641.5 eV, and 5 main peaks were assigned to this signal, ranging from 640–643.9 eV. This range is close to the analyses from earlier research on natural manganite and in-vacuum fractured mineral specimens of manganite,[39,33] with deviations of less than 1 eV. Similar to the other materials, 3 peaks were assigned to the O 1s spectrum. The two major peaks at 529.6 and 530.8 eV represent the contributions from O^{2-} and OH^- respectively. Near-identical contributions were observed for these 2 chemical environments as well, suggesting their equal abundance in this material. A small but broad signal at the higher binding energy side (~533 eV) may be due to chemisorbed or structurally bound water present in negligible amounts.[35,37] It is mentionable that this peak might be a representation of another hydroxide which is structurally different from the MnO(OH) hydroxide environment.

NiO(OH) Finally, the Ni 2p and O 1s spectra for NiO(OH) are presented in Figure 4E. Like in earlier investigations,[40] the characteristic $2p_{3/2}$ signal falls in the region from about 853–864 eV with 7 peaks assigned to it. This $2p_{3/2}$ spectrum, like the Mn 2p spectrum, fits well with the Ni^{3+} free ion multiplet proposed by Gupta and Sen, which contains 6 prominent

peaks.[38] The additional peak observed in Figure 4E (left) at around 857 eV might be due to presence of trace amounts of Ni^{2+} ions, as supported in a previous study by Grosvenor *et. al,*[41] This attribution is further confirmed by the O 1s spectrum, where the ratio of OH^{-}:O^{2-} (at 531.7 and 529.2 eV respectively) is 2:1 instead of the ideal 1:1 in the event where these two groups are present in equivalent abundance. This further suggests the existence of a mixed Ni^{2+}/Ni^{3+} phase in the NiO(OH) synthesized in this work, or particularly decomposition of NiO(OH) to $Ni(OH)_2$.2NiO(OH) as proposed previously.[41] Nonetheless, the mean Ni $2p_{3/2}$ binding energy of about 857 eV concurs largely with literature value for Ni (III) compounds, and confirming the results of X-ray diffraction where the mixed valence state was confirmed as a phase $3Ni(OH)_2$.NiO(OH).

The inherent electrochemistry of the five layered oxyhydroxides, involving the oxidation and reduction peaks of the respective materials, were subsequently examined in phosphate buffer solution purged with nitrogen, and shown in **Figure 5**. Anodic signals were more apparent at approximately +0.8 V for cobalt and manganese oxyhydroxides (Figures 5A and D); slight oxidation signals were also observed for the other three materials. Other than more evident reduction signals at about –1.0 V which denote the reduction of possible oxygen in the PBS electrolyte, CoO(OH) and NiO(OH) exhibited a second prominent reduction peak near +0.9 V. Slight reduction signals were also evident for the other three materials, at around 0 V. These oxidation and reduction peaks are likely to represent the Ni^{2+}/Ni^{3+} redox schemes. Nonetheless, intrinsic electrochemistry was more prominent in CoO(OH) and NiO(OH), deeming them more electroactive than their counterparts at a preliminary stage.

Electrocatalytic capability of the five layered oxyhydroxides was first explored using hydrogen evolution reaction in acidic medium. The progress of hydrogen evolution for the materials, together with platinum and bare GC surfaces as references, is shown in **Figure 6A**. Among the layered oxyhydroxides, onset of HER took place earliest for CoO(OH) and NiO(OH) at around –0.8 V, and latest for MnO(OH) at around –1.1 V. Platinum-coated surface shows the best electrocatalytic performance, with HER occurring at approximately –0.1 V. Despite their inferiority against platinum, proton reduction occurred earlier for most of the oxyhydroxides as compared to the bare GC surface. **Figure 6B** summarises the potential at which the current density reaches –10 mA cm^{-2}, an estimated value 10 % efficiency of a solar-to-fuel device.[42] This current density value was achieved at the earliest potential for Pt/C as predicted. In terms of the five layered oxyhydroxides, CoO(OH) and NiO(OH) achieved a current density of –10 mA cm^{-2} earliest at less than –0.9 V, whereas this value took place at close to –1.3 V for MnO(OH), later than that for bare GC (–1.2 V). To further affirm the electrocatalytic potential of the

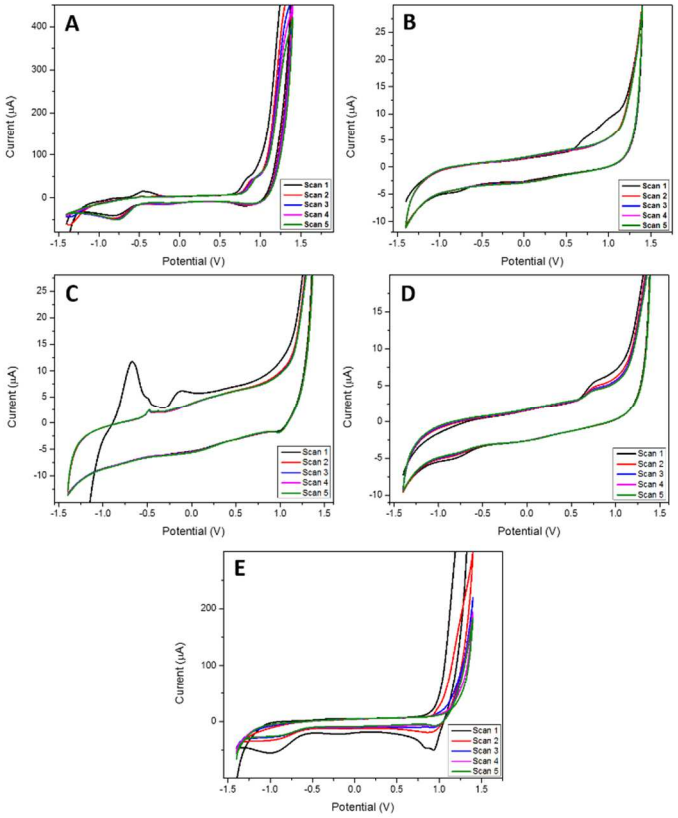

Figure 5 Cyclic voltammograms of PBS background electrolyte (50 mM, pH 7.2) on (A) CoO(OH), (B) CrO(OH), (C) FeO(OH), (D) MnO(OH) and (E) NiO(OH) surfaces for five consecutive scans in the anodic direction. Scan rate: 100 mV s^{-1}.

materials, Tafel slope values were then calculated. The Tafel slope indicates the increase of the overpotential required in order to raise the current density by 10-fold. A smaller increase in overpotential, as represented by a smaller Tafel slope value, would mean a more efficient HER.

The Tafel slope, along with the slope values are displayed in **Figures 7A** and **7B** respectively. NiO(OH) exhibits the best electrocatalytic behaviour out of the five layered oxyhydroxides, with a Tafel slope value of about 62 mV/dec. This value is closest to that of Pt/C, which generated a Tafel value of 34 mV/dec, a better result as compared to other nickel-based materials investigated formerly.[43,44] The performance of NiO(OH) is closely followed by CoO(OH), which gave a small Tafel value of about 87 mV/dec. Tafel values of CrO(OH) and FeO(OH) were between 100 and 150 mV/dec; out of all the materials including the bare GC surface, MnO(OH) was the most inferior in terms of Tafel slope value. Based on the parameters studied above, CoO(OH) and NiO(OH) appear to be the most promising catalysts in the generation of hydrogen. This observation can be ascribed to the 'volcano' plot which positions different metals based on their hydrogen adsorption energies, ΔG_H.[10,45] Ideal electrocatalysts for HER have a ΔG_H value very close to 0, where hydrogen is neither bound too strongly or weakly to the electrode surface. Nickel and cobalt have ΔG_H values of about –0.25 eV, which is near to that of platinum and palladium. As such, the rate of the hydrogen

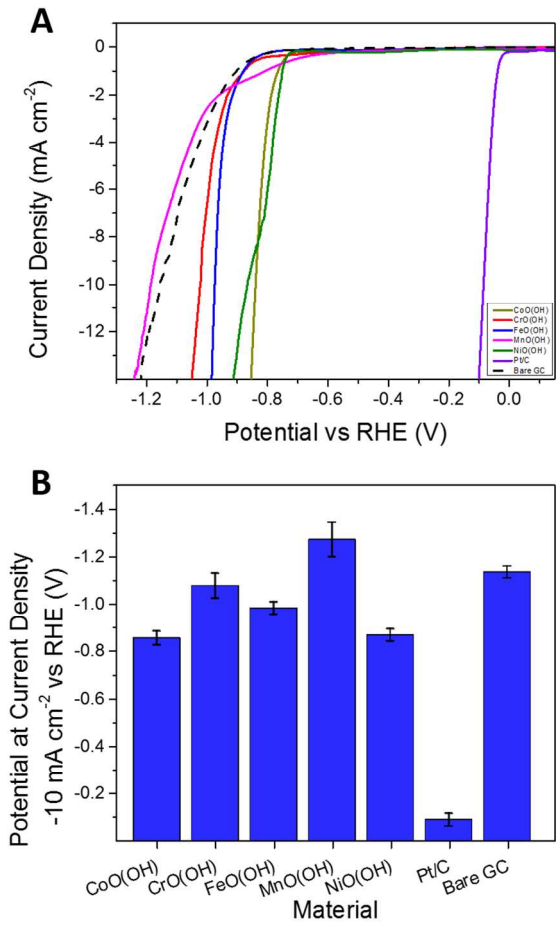

Figure 6 (A) Linear sweep voltammograms of hydrogen evolution and (B) current density of the seven surfaces at overpotential of –10 mV. Conditions: 0.5 M sulfuric acid, scan rate 2 mV s^{-1}.

evolution, mainly dependent on the ΔG_H, is believed to be higher for materials comprising of these two metals. The stability of oxyhydroxides in alkaline environment is very high with exception of CrO(OH) which have amphoteric behaviour and can form complex hydroxochromium anions. In the acidic environment (0.5M H_2SO_4) have oxohydroxides of Cr, Mn, Fe and Co relatively good stability while nickel oxohydroxides tend to dissolve in several hours with simultaneous reduction on Ni^{2+} and oxygen evolution.

The layered oxyhydroxides were next examined with respect to OER, the second process in water-splitting. OER is more kinetically demanding as compared to HER, due to more number of steps involved, as well as the need for four redox equivalents per turnover to form molecular oxygen.[46] The oxygen evolution curves of the materials were compared with the bare GC surface and presented in **Figure 8A**. It is evident that only CoO(OH) and NiO(OH) were able to achieve a current density of 10 mA cm^{-2} (at around +1.8 V), an important indication of the material's catalytic ability in energy conversion. Onset of oxygen evolution took place at about +1.6 V for both materials, which is analogous to other cobalt- and nickel-based catalysts.[47,48] Tafel slopes were evaluated for the materials as well, and encapsulated in **Figure 8B**. CoO(OH) and NiO(OH) generated Tafel slopes of 55 and 144 mV/dec respectively; The performance of the former is relatively close to the 40 mV/dec attained by IrO_2. As broad inherent signals were observed for CrO(OH), FeO(OH) and MnO(OH), the water-splitting portion might be masked, resulting in skewed

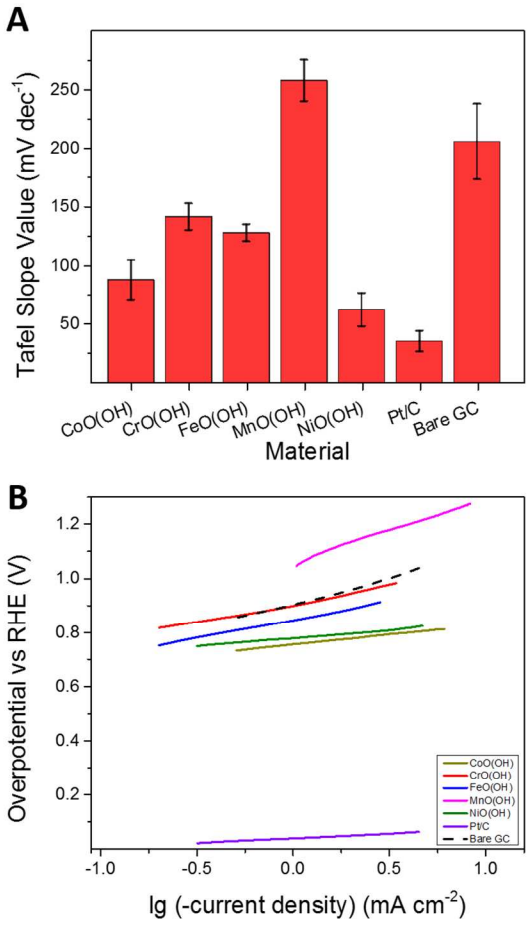

Figure 7 (A) Tafel slopes of hydrogen evolution on the seven surfaces and (B) their respective Tafel slope values.

Tafel data which was only collected after the intrinsic signal. These materials and the bare GC surface evidently failed to provide electrocatalytic effect towards OER. From our study, only CoO(OH) and NiO(OH) can fit the demanding criteria of an OER catalyst out of the five layered oxyhydroxides studied.

The electrocatalytic potentials of the oxyhydroxides were lastly assessed using oxygen reduction reaction. Peak current of about 18 µA was obtained for NiO(OH), as illustrated by the voltammograms in **Figure 9A**. Dotted curves in Figure 9A represent the same reaction carried out in potassium hydroxide purged with nitrogen. Absence of signals show that the reduction peaks obtained for the solid-lined curves represent the reduction of saturated oxygen in the analyte. This comparison is indicative of the catalytic abilities of the layered hydroxides for ORR. **Figure 9B** presents the analysis of the second parameter, onset potential of the reaction with the various surfaces. The onset potential is determined by extracting the potential value at

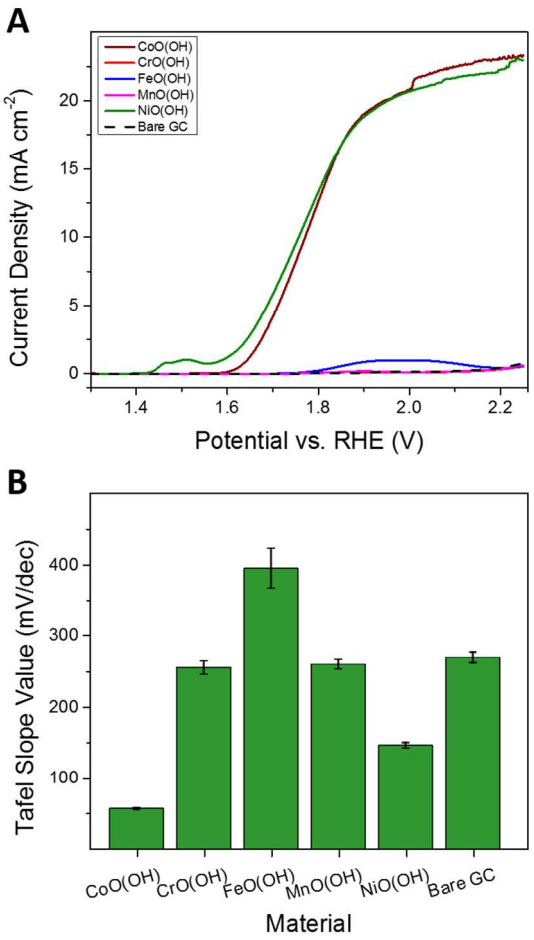

Figure 8 (A) Linear sweep voltammograms of oxygen evolution and (B) Tafel slope values of the six surfaces. Conditions: 0.1 M potassium hydroxide, scan rate 2 mV s^{-1}.

which 10 % of the peak current value takes place. Unsurprisingly, onset potential for ORR is the lowest at Pt/C at about –0.06 V. As for the five oxyhydroxides, their onset potentials ranged from –0.25 V to –0.33 V, with the earliest onset potential coming from CoO(OH) and the largest overpotential needed at NiO(OH).

4. Conclusions

Layered metal oxyhydroxides is a group of materials underexplored other than recent studies on their catalytic effects on OER application. This work investigated the electrochemistry of layered oxyhydroxides of five metals, cobalt, chromium, iron, manganese and nickel and their potentials as electrocatalysts in three significant energy-related applications (HER, OER and ORR) after respective syntheses and characterisations. While the materials were inferior to platinum and iridium in the respective applications, they have demonstrated electrocatalytic capabilities to a certain extent. The analyses suggested that CoO(OH) and NiO(OH) appear to be more promising than the other three layered materials, as well as the bare GC surface. This is especially evident in the case of HER and OER, where the kinetics of these two reactions were greatly enhanced, deeming CoO(OH) and NiO(OH) promising electrocatalyst alternatives. As our world progresses towards a cleaner approach for energy development, these cost-effective and earth-abundant materials would definitely be useful alternatives in generating sustainable and recyclable energy carriers.

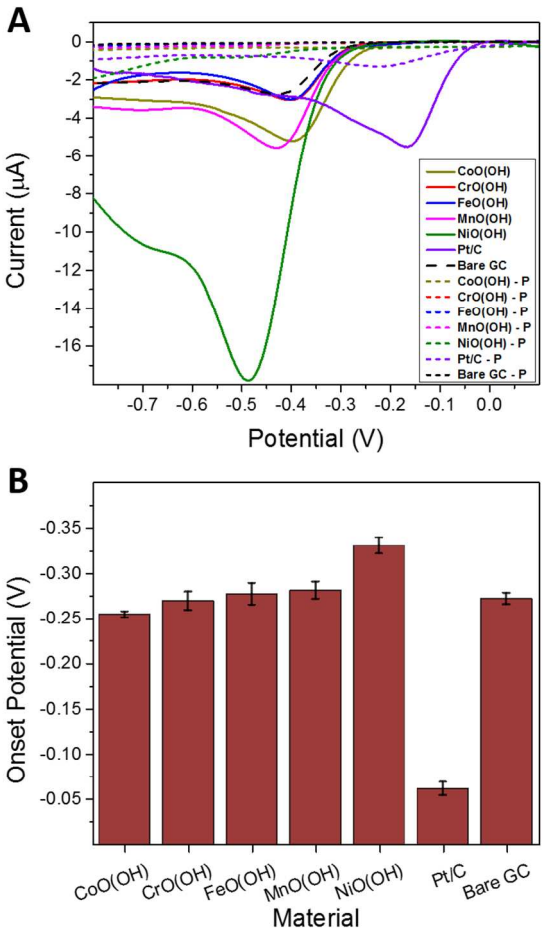

Figure 9 (A) Linear sweep voltammograms of oxygen reduction in the presence and absence of saturated oxygen and (B) onset potential values of the seven surfaces. Conditions: 0.1 M potassium hydroxide, scan rate 5 mV s^{-1}.

Acknowledgment

M.P. acknowledges a Tier 2 grant (MOE2013-T2-1-056; ARC 35/13) from the Ministry of Education, Singapore. Z.S. and K.K. were supported by Specific university research (MSMT no. 20/2015) and Czech Science Foundation (GACR no. 13-17538S). The research leading to these results received funding from the European Union Seventh Framework Programme under Grant Agreement 312483 - ESTEEM2 (Integrated Infrastructure Initiative–I3).

Notes and references

[a] School of Physical and Mathematical Science, Division of Chemistry and Biological Chemistry, Nanyang Technological University, 21 Nanyang Link, Singapore. Email: pumera.research@gmail.com

[b] Department of Inorganic Chemistry, University of Chemistry and Technology Prague, Technická 5, 166 28 Prague 6, Czech Republic.
[c] Ernst Ruska-Centrum and Peter Grünberg Institute, Forschungszentrum Jülich, 52425 Jülich, Germany.

1 X. Long, J. Li, S. Xiao, K. Yan, Z. Wang, H. Chen and S. Yang, *Angew. Chem. Int. Ed.*, 2014, **126**, 7714.
2 D. Merki and X. Hu, *Energy Environ. Sci.*, 2011, **4**, 3878.
3 J. Barber, *Chem. Soc. Rev.*, 2009, **38**, 185.
4 M. G. Walter, E. L. Warren, J. R. McKone, S. W. Boettcher, Q. X. Mi, E. A. Santori and N. S. Lewis, *Chem. Rev.*, 2010, **110**, 6446.
5 T. Abbasi, S. Abbasi, *Renewable Sustainable Energy Rev.*, 2011, **15**, 3034.
6 B. E. Conway and B. V. Tilak, *Electrochim. Acta.*, 2002, **47**, 3571.
7 J. Greeley, T. F. Jaramillo, J. Bonde, I. B. Chorkendorff and J. K. Nørskov, *Nat. Mater.*, 2006, **5**, 909.
8 J. Rosen, G. S. Hutchings and F. Jiao, *J. Am. Chem. Soc.*, 2013, **135**, 4516.
9 P. M. Vignais, B. Billoud and J. Meyer, *FEMS. Microbiol. Rev.*, 2001, **25**, 455.
10 J. D. Benck, T. R. Hellstern, J. Kibsgaard, P. Chakthranont and T. F. Jaramillo, *ACS Catal.*, 2014, **4**, 3957.
11 I. Zaharieva, M. M. Najafpour, M. Wiechen, M. Haumann, P. Kurz and H. Dau, *Energy Environ. Sci.* 2011, **4**, 2400.
12 M. W. Louie and A. T. Bell, *J. Am. Chem. Soc.*, 2013, **135**, 12329.
13 J. A. Koza, Z. He, A. S. Miller and J. A. Switzer, *Chem. Mater.*, 2012, **24**, 3567.
14 C. Jin, F. L. Lu, X. C. Cao, Z. R. Yang and R. Z. Yang, *J. Mater. Chem. A*, 2013, **1**, 12170.
15 K. Ariga, Y. Yamauchi, G. Rydzek, Q. Ji, Y. Yonamine, K. C.-W. Wu and J. P. Hill, *Chem. Lett.*, 2014, **43**, 36.
16 R. Ma and T. Sasaki, *Acc. Chem. Res.*, 2015, **48**, 136.
17 I. D. Welsh and P. M. A. Sherwood, *Phys Rev B,* 1989, **40**, 6386.
18 L. Liu, Z. Zhou and C. Peng, *Electrochim. Acta.*, 2008, **54**, 434.
19 W. Ma, R. Ma, C. Wang, J. Liang, X. Liu, K. Zhou and T. Sasaki, *ACS Nano*, 2015, **9**, 1977.
20 Y. Miao, L. Ouyang, S. Zhou, L. Xu, Z. Yang, M. Xiao and R. Ouyang, *Bionsens. Bioelectron.*, 2014, **53**, 428.
21 J. A. Seabold and K.-S. Choi, *J. Am. Chem. Soc.*, 2012, **134**, 2186.
22 Y.-C. Liu, J. A. Koza and J. A. Switzer, *Electrochim. Acta.*, 2014, **140**, 359.
23 L. Trotochaud, S. L. Young, J. K. Ranney and S. W. Boettcher, *J. Am. Chem. Soc.*, 2014, **136**, 6744.
24 T. W. Kim and K.-S. Choi, *Science*, 2014, **343**, 990.
25 X. Ren, S. S. Zhang, D. T. Tran and J. Read, J. *J. Mater. Chem.*, 2011, **21**, 10118.
26 X. Wang, P. J. Sebastian, M. A. Smit, H. Yang and S. A. Gamboa, *J. Power Sources*, 2003, **124**, 278.
27 J. Yang, H. Liu, W. N. Martens and R. L. Frost, *J. Phys. Chem. C*, 2010, **114**, 111.
28 N. S. McIntyre and M. G. Cook, *Anal. Chem.*, 1975, **47**, 2208.
29 J. Stoch and J. Gablankowska-Kukucz, *Surf. Interface Anal.*, 1991, **17**, 165.
30 I. Ikemoto, K. Ishii, S. Kinoshita, H. Kuroda, M. A. A. Franco and J. M. Thomas, *J. Sol. State Chem.*, 1976, **17**, 425.
31 J. Yang, A. G. Baker, H. Liu, W. N. Martens and R. L. Frost, *J. Mater. Sci.*, 2010, **45**, 6574.
32 G. C. Allen, M. T. Curtis, A. J. Hooper and P. M. Tucker, *Dalton Trans.*, 1973, 1675.
33 M. C. Biesinger, B. P. Payne, A. P. Grosvenor, L. W. M. Lau, A. R. Gerson and R. St. C. Smart, *Appl. Surf. Sci.*, 2011, **257**, 2717.
34 T.-C. Lin, G. Seshadri and J. A. Kelber, *Appl. Surf. Sci*., 1997, **119**, 83.
35 N. S. McIntyre and D. G. Zetaruk, *Anal. Chem.*, 1977, **49**, 1521.
36 S. Suzuki, K. Yanagihara and K. Hirokawa, *Surf. Interface Anal.*, 2000, **30**, 372.
37 A. R. Pratt, I. J. Muir and H. W. Nesbitt, *Geochimica et Cosmochimica Acta.*, 1994, **58**, 827.
38 R. P. Gupta and S. K. Sen, *Phys. Rev. B*, 1975, **12**, 15.
39 H. W. Nesbitt and D. Banerjee, *Am. Mineral.*, 1998, **83**, 305.
40 M. C. Biesinger, B. P. Payne, L. W. M. Lau, A. Gerson, A and R. St. C. Smart, *Surf. Interface Anal.,* 2009, **41**, 324.
41 A. P. Grosvenor, M. C. Biesinger, R. St. C. Smart and N. S. McIntrye, *Surf. Sci.*, 2006, **600**, 1771.
42 C. R. Cox, J. Z. Lee, D. G. Nocera and T. Buonassisi, *PNAS*, 2014, **111**, 14057.
43 W-F. Chen, K. Sasaki, C. Ma, A. I. Frenkel, N. Marinkovic, J. T. Muckerman, Y. Zhu and R. R. Adzic, *Angew. Chem. Int. Ed.*, 2012, **51**, 6131.
44 E. Navarro-Flores, Z. Chong and S. Omanovic, *J. Mol. Catal. A*, 2005, **226**, 179.
45 J. K. Nørskov, T. Bligaard, A. Logadottir, J. R. Kitchin, J. G. Chen, S. Pandelov and U. Stimming, *J. Electrochem. Soc.*, 2005, **152**, J23.
46 R. Eisenberg and H. B. Gray, *Inorg. Chem.*, 2008, **47**, 1697.
47 X. Li, F. C. Walsh and D. Pletcher, *Phys. Chem. Chem. Phys.*, 2011, **13**, 1162.
48 L. Trotochaud, J. K. Ranney, K. N. Williams and S. W. Boettcher, *J. Am. Chem. Soc.*, 2012, **134**, 17253.

